Electrostatics of the protein-water interface and the dynamical transition in proteins

Dmitry V. Matyushov and Alexander Y. Morozov

Phys. Rev. E **84**, 011908 — Published 14 July 2011

DOI: 10.1103/PhysRevE.84.011908

Electrostatics of the protein-water interface and dynamical transition in proteins

Dmitry V. Matyushov* and Alexander Y. Morozov
Center for Biological Physics, Arizona State University, PO Box 871604, Tempe, AZ 85287-1604

Atomic displacements of hydrated proteins are dominated by phonon vibrations at low temperatures and by dissipative large-amplitude motions at high temperatures. A crossover between the two regimes is known as a dynamical transition. Recent experiments indicate a connection between the dynamical transition and the dielectric response of the hydrated protein. We analyze two mechanisms of the coupling between the protein atomic motions and the protein-water interface. The first mechanism considers viscoelastic changes in the global shape of the protein plasticized by its coupling to the hydration shell. The second mechanism involves modulations of the local motions of partial charges inside the protein by electrostatic fluctuations. The model is used to analyze mean square displacements of iron of metmyoglobin reported by Mössbauer spectroscopy. We show that high displacement of heme iron at physiological temperatures is dominated by electrostatic fluctuations. Two onsets, one arising from the viscoelastic response and the second from electrostatic fluctuations, are seen in the temperature dependence of the mean square displacements when the corresponding relaxation times enter the instrumental resolution window.

PACS numbers: 87.14.E-, 87.15.H-, 87.15.kr, 87.10.Pq
Keywords: Dynamical transition, Mössbauer spectroscopy, hydrated protein, electrostatic fluctuations.

I. INTRODUCTION

Measurements of the Mössbauer absorption of ^{57}Fe in metmyoglobin crystals revealed that the mean square displacement (msd) of this atom starts to grow faster with increasing temperature above $T_d \simeq 200$ K [1]. This finding was followed by similar observations from neutron scattering [2], which by now have been reported for a large number of proteins and other biopolymers [3], all demonstrating the same phenomenology [4–6]. The increase in the slope of the protein msd as a function of temperature was called a "dynamical transition", presently assigned to a rather broad range of onset temperatures $T_d \simeq 200-240$ K. The basic observation is that the high-temperature msd of proteins much exceeds the linear extrapolation of the low-temperature behavior characteristic of a solid. The low-temperature portion of the msd is well characterized by the observed phonon spectrum of the protein [7], while the high-temperature msd excess is linked to dissipative long-wavelength modes with energies below $\simeq 4$ meV [8–11].

Early explanations of the dynamical transition offered scenarios ranging from detrapping of the protein conformational motions from low-energy states [7, 12, 13] to the glass transition in bulk water [2]. Several recent observations have shifted the focus to the protein-water interface and, in particular, to the protein's hydration shell. Two observations are particularly important here: (i) the disappearance of the dynamical transition in dry protein powders [14] and (ii) its separate existence for the hydration water [15–17]. Both results point to a strong link between the atomic msd of groups buried inside the protein and the coupled surface fluctuations of the hydration shell and the protein. We indeed show in this paper that the msd excess at high temperatures is caused by electrostatic fluctuations produced by polar/charged groups at the protein surface and water molecules residing in the protein's first hydration shell.

Despite somewhat different semantics, the views in the field seem to converge to the notion of the critical role of the hydration shell in promoting the dynamical transition. According to Doster [18]: "The onset of the dynamical transition depends on the solvent viscosity near the protein surface.... The protein-water α-process consists of a concerted librational motion of protein surface residues, coupled to translational jumps of water molecules on the same time scale." The physical mechanism behind the transition is assigned in this view to the caging of the protein by water's hydrogen bonds, stiffening its conformational flexibility. As the temperature increases, the population of broken hydrogen bonds grows exponentially, resulting in a release of the protein conformational flexibility in a narrow range of temperatures. Although appealing, this concept does not address the key question of how $\sim 0.5-2$ ps local events of hydrogen bond breaking develop into a $\sim 2\mu$s (Ref. 19) collective α-relaxation at T_d.

Frauenfelder and co-workers have recently suggested a somewhat different scenario, also focusing on the dynamics of the protein hydration shell [20–23]. According to their view, protein internal motions (but not large-scale conformational changes) are coupled to the motions of interfacial waters and their dynamics are dominated by the dynamics of the hydration layer. The corresponding relaxation times follow an Arrhenius law and are therefore classified as a secondary, β-process in analogy with the common classification adopted in the field of supercooled liquids [24]. This secondary relaxation of the hydration shell is therefore distinguished from the primary, α-relaxation bulk water. The latter shows non-Arrhenius

* dmitrym@asu.edu

temperature dependence on cooling [24]. The β-process of the hydration shell, and its effect on internal protein motions, is experimentally separated from the bulk water dynamics by embedding protein samples into solid poly(vinyl)alcohol (PVA). The dynamics of β-relaxation is then measured by dielectric spectroscopy [21, 22].

The use of dielectric absorption of PVA-confined proteins yields a surprisingly accurate account of the temperature dependence of the Lamb-Mössbauer factor equal to the fraction of recoilless absorption, $f = \exp[-k_0^2\langle(\delta x)^2\rangle]$. Here, $\langle(\delta x)^2\rangle$ is the msd of the heme iron of metmyoglobin in projection on the wavevector $\mathbf{k}_0$ of γ-radiation. The iron msd can be separated into a vibrational, low-temperature component $\langle(\delta q)^2\rangle \propto T$, described by the vibrational density of states (VDOS) of the protein, and a high-temperature component $\langle(\delta Q)^2\rangle$ appearing at $T > T_d$. Since the $\mathbf{q}$ and $\mathbf{Q}$ coordinates are typically considered as statistically independent [10, 22, 25, 26], $f = f_q f_Q$ becomes a product of two components, f_q and f_Q. It turns out that, once the extrapolation of the low-temperature component f_q is subtracted from the observed signal, the temperature variation of f_Q is exceptionally well reproduced by the variance of the sample dipole moment at the same hydration level

$$f_Q = \exp[-k_0^2\langle(\delta Q)^2\rangle] = \langle(\delta M)^2\rangle_< / \langle(\delta M)^2\rangle. \qquad (1)$$

In this equation, $\langle(\delta M)^2\rangle_<$ is defined as the integral of the frequency-dependent variance of the sample dipole moment M_ω over the frequencies below (subscript "<") the instrumental frequency $\omega_{\rm obs} = 1/\tau_{\rm obs}$, $\tau_{\rm obs} = 140$ ns [22]. The parameter f_Q then determines the fraction of the sample dipole that has not had a chance to alter on the life-time of the iron nucleus, thus keeping the nuclei in resonance for Mössbauer absorption.

The empirical connection between the dynamical transition and dipolar fluctuations is additionally supported by recent observations of breaks in the dependence of the terahertz dielectric absorption on temperature at typical values of T_d [27]. All these observations, although advancing the field toward identifying the physical modes responsible for the high-temperature flexibility of proteins [13], pose a significant conceptual challenge.

Both Mössbauer and neutron-scattering techniques probe translational atomic motions on their corresponding resolution windows. It seems therefore natural to relate the break in the temperature dependence of the msd to changes in the dynamic and/or static properties of atomic translations [28, 29]. This is the conceptual framework behind the glass-transition scenario [18] which, even in the current form emphasizing the hydration layer, is focused on the caging arrest, i.e., on the primary effect of short-ranged repulsive interactions in the system. On the contrary, the dielectric measurements [22, 27, 30] shift the focus to the long-ranged dipolar fluctuations.

Translational (density) and orientational (dipolar polarization) modes are mostly decoupled by symmetry and can therefore be considered as two distinct mechanisms of altering the protein atomic msd [31]. Numerical simulations find enhanced fluctuations of hydrogen bonds of hydration water at high temperatures [28], but those can be projected on either density or collective orientational modes. The common temperature dependence of the response produced by atomic translations of groups buried inside the protein and dipolar orientations predominantly active at the protein-water interface [23, 32–34] suggests a common physical property linking the two modes. We show here that this property is the electric field of the protein-water interface acting on an atomic charge inside the protein.

The goal of this paper is to develop a model of the protein atomic msd based on the properties of the protein-water interface. Low-frequency deformations of the protein-water interface, not included in the phonon VDOS, are modeled here by the viscoelastic response function and the interfacial electrostatics are modeled by the response function of the electric field acting on buried atomic charges. The dependence of the onset temperature T_d on the observation window is an important ingredient of the observations [18, 35], which is introduced into the theory by limiting the range of frequencies over which the response functions are integrated [36], similarly to Eq. (1). We start with formulating the model, followed by the results of calculations.

II. MODEL

The purpose of our model is to determine the msd of a single atom, heme iron of metmyoglobin, as a function of temperature. The atomic msd mostly originates from projections of normal mode vibrations of the protein on the atomic displacement, iron in our case. This component, described by the vibrational coordinate $\mathbf{q}$, can be directly calculated from the VDOS measured, for instance, by the phonon-assisted Mössbauer scattering [7, 26, 37]. Its msd is, in the classical limit, a linear function of temperature shown by the dashed line in Fig. 1

$$\langle(\delta q)^2\rangle(T) = a_q T. \qquad (2)$$

The proportionality coefficient a_q is calculated from the VDOS according to the standard prescriptions [26].

We show below that the interaction of the atomic charge of the heme iron with the local electric field of the protein-water interface results in softening of the atomic vibrations. This effect is recorded by the experimental $\langle(\delta x)^2\rangle(T)$ as an increase of its slope vs temperature as shown by closed points in Fig. 1. The solid line in Fig. 1 is the result of the calculation incorporating this electrostatic softening using model parameters in agreement with Molecular Dynamics (MD) simulations (see below). The break in the slope of $\langle(\delta x)^2\rangle(T)$ at T_d occurs when the relaxation time of the electric field fluctuations enters the experimental observation window of Mössbauer spectroscopy, $\tau_{\rm obs} = 140$ ns [22].

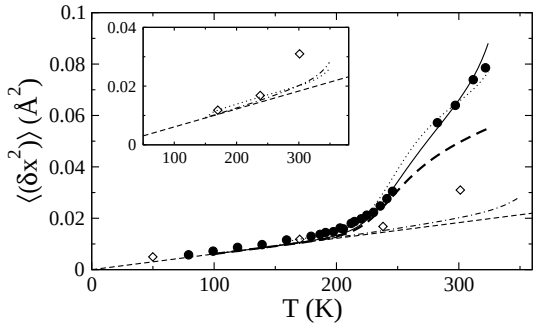

FIG. 1. Temperature dependence of the iron msd in metmyoglobin. Experimental msd [7] are shown by circles. Diamonds refer to the msd calculated from the VDOS measured from phonon-assisted Mössbauer effect at different temperatures [7], whereas the dashed line is the same calculation from the VDOS at 235 K [26]. The dash-dotted line refers to $\langle(\delta x^2)\rangle_{\rm el}$ [Eq. (11)] combining phonons with viscoelastic oscillations of the protein shape. The solid line refers to the combination of all three effects: protein's phonons, viscoelastic shape oscillations, and electrostatic fluctuations [Eq. (10)]. Further, the bold dashed line refers to the calculation neglecting the viscoelastic component $\langle(\delta Q)^2\rangle_>$ in the elastic msd in Eq. (11). The inset shows vibrational msd $\langle(\delta q)^2\rangle$ (dashed line) and elastic msd $\langle(\delta x^2)\rangle_{\rm el}$ (dash-dotted and dotted lines). The solid line in the main panel is obtained with $\Delta K_p(T)$ as explained in the text, while the dotted lines in both panels refer to the temperature-independent $\Delta K_p = 3.2$ GPa obtained from the fit of Eq. (16) to the protein intrinsic compressibility at 298 K [38].

While the theory advanced here suggests that $\langle(\delta q)^2\rangle(T)$ and its softening by the local electric field of the protein-water interface are two major components required to reproduce the experimental $\langle(\delta x)^2\rangle(T)$, one also wonders what are the effects of global viscoelastic deformations of the protein shape on the atomic msd. This problem unfortunately cannot be currently resolved with atomic or even coarse-grained resolution. While approaches to study global motions of proteins by coarse-grained models (e.g., elastic network models [39–42]) have been successfully advanced in recent years, the solution of a viscoelastic analog of this approach still lags behind. This is the result of both the difficulties of solving the viscoelastic problem [43] for objects of complex shape and the absence of established dynamic moduli of proteins of which only the static compressibility has been sufficiently studied [38, 44].

In order to provide estimates of the effect of global viscoelastic shape fluctuations on the iron msd, we develop here a formalism limited to a simplified spherical geometry thus including only the projections of the global low-frequency deformations of the protein on the radial expansion of the protein volume for which the bulk modulus is sufficient. The model is parametrized on the experimental volumetric data and shows that viscoelastic motions become important at high temperatures. The bold dashed line in Fig. 1 was obtained by neglecting the viscoelastic deformations altogether, and the resulting msd falls below the experimental points by $\simeq 30\%$.

We will split the coordinate of the iron atom $\mathbf{r} = \mathbf{q}+\mathbf{Q}$ into two statistically independent components, $\mathbf{q}$ and $\mathbf{Q}$ [25]. The dissipative motions of the protein, described by coordinate $\mathbf{Q}$, are seen in neutron scattering spectra as a quasielastic peak with energies below $\simeq 4$ meV, growing in intensity with increasing temperature [10]. In contrast, high-frequency vibrations projecting on the $\mathbf{q}$-coordinate produce a temperature independent scattering intensity. Further, with the sound velocity of a protein $\simeq 1700$ m/s [9, 45], the wavelength of the corresponding Q-modes is about 26 Å, which is comparable with the diameter of myoglobin, $2R = 36$ Å. These modes therefore alter the global shape of the protein, which is the domain of the viscoelastic response.

The protein viscoelastic motions are modeled as radial vibrations of a sphere of radius R immersed in a viscoelastic water continuum. The low-frequency iron msd is then related to the radius fluctuations of the sphere as $\langle(\delta Q^2)\rangle = (r/R)^2\langle(\delta R)^2\rangle$. The latter can be found by solving the standard equations of viscoelasticity [43, 46] yielding the response function $\chi_R(\omega)$ connecting the change of the sphere's radius R to an oscillatory pressure $p(t) = p_0 e^{i\omega t}$ applied to the sphere's surface. The result is [46]

$$\chi_R(\omega) = -\frac{1}{4\pi R}\frac{1}{3\Delta K_p(\omega) + 4\mu_w(\omega)}. \qquad (3)$$

Here, $\Delta K_p(\omega) = K_p(\omega) - K_{p,0}$ is the viscoelastic bulk modulus of the protein minus its bulk modulus $K_{p,0}$ at zero frequency. Further, $\mu_w(\omega)$ is the shear modulus of water. Applying the fluctuation-dissipation theorem [47] to Eq. (3), one gets

$$\langle(\delta Q_\omega)^2\rangle = -\frac{2k_{\rm B}Tr^2}{3\omega V_p}{\rm Im}\frac{1}{3\Delta K_p(\omega) + 4\mu_w(\omega)}, \qquad (4)$$

where V_p is the protein volume.

We now proceed to calculating the Lamb-Mössbauer factor [48–50]

$$f = \langle\left|\langle e^{ik_0 x}\rangle\right|^2\rangle_{\rm het}, \qquad (5)$$

where $x = \hat{\mathbf{k}}_0\cdot(\mathbf{q}+\mathbf{Q})$ is the projection of the iron displacement on the direction of photon propagation, $\hat{\mathbf{k}}_0 = \mathbf{k}_0/k_0$. There are two averages in this definition: the inner angular brackets denote the canonical ensemble average over the protein and water modes affecting the position of iron in a single protein, while the outer angular brackets denote an average over the proteins in the sample. This second average carries the subscript "het" to emphasize that it reflects the heterogeneity of the sample, such as for instance variations in the hydration level among different proteins in the protein powder. We do not consider the heterogeneous average in our present study and limit ourselves by the inner average only. This approximation amounts, in experimental techniques, to

considering the narrow feature of the Mössbauer absorption line and subtracting the broad base-line originating from the sample heterogeneity [7]. Accordingly, the experimental closed points shown in Fig. 1 are obtained from the area $f(T)$ of the narrow line as $-\ln f(T)/(k_0)^2$, $k_0 = 53.2$ Å^{-1}.

One has to recognize that the distinction between the heterogeneous average in the outer brackets and the canonical average in the inner brackets in Eq. (5) is not clearly specified. The canonical average includes only the modes of the medium with relaxations times $\tau(T)$ faster than the instrumental observation window $\tau_{\rm obs}$. This fact will be explicitly incorporated below in all response functions of the slow modes by restricting the integrals over the mode frequencies by fast modes only [36]. However, once the temperature is lowered, an increasing fraction of the phase space sampled by water and conformational motions of a single protein falls outside the canonical average and thus should be included in the heterogeneous average in the outer brackets in Eq. (5). This component of the picture is completely neglected here, but needs to be considered to incorporate the broad base-line feature of Mössbauer band-shapes [7, 48–50].

The canonical ensemble average over the water/protein statistical distribution can be described in terms of the free energy $F(x)$ such that the inner brackets in Eq. (5) become

$$\langle e^{ik_0 x}\rangle = Z^{-1}\int e^{ik_0 x-\beta F(x)}dx, \tag{6}$$

where $\beta = 1/(k_{\rm B}T)$ and $Z = \int \exp[-\beta F(x)]dx$. The free energy $F(x)$ is determined by projecting [51] the manifold of $\mathbf{q}$ and $\mathbf{Q}$ coordinates on the single coordinate x

$$e^{-\beta F(x)} = \int \delta[x-\hat{\mathbf{k}}_0\cdot(\mathbf{q}+\mathbf{Q})] \langle e^{-\beta H_0(\mathbf{q},\mathbf{Q})-\beta z\phi_w(\mathbf{q},\mathbf{Q})}\rangle_w \; d\mathbf{q}d\mathbf{Q}. \tag{7}$$

In this equation, $H_0(\mathbf{q},\mathbf{Q})$ is the Hamiltonian of classical harmonic vibrations of the protein and ϕ_w is the electrostatic potential of the dielectric medium acting on the heme iron with the charge z. The subscript "w" in Eq. (7) specifies water as the main source of the electrostatic fluctuations. This is, however, not required by the theory, and slow protein motions, not included in the calculation of $\langle(\delta q)^2\rangle$, can contribute to the fluctuations of the electrostatic potential as well (see below). In that case, ϕ_w denotes the overall electrostatic potential arising from the heterogeneous, protein-water medium surrounding the heme.

The Hamiltonian $H_0(\mathbf{q},\mathbf{Q})$ in Eq. (7) can be given in the Gaussian form

$$\beta H_0(\mathbf{q},\mathbf{Q}) = \frac{\delta q^2}{2\langle(\delta q)^2\rangle} + \frac{\delta Q^2}{2\langle(\delta Q)^2\rangle_>}, \tag{8}$$

where the variance of $\mathbf{q}$ is given by Eq. (2) and the variance of $\mathbf{Q}$ requires additional explanation.

The limited instrumental time $\tau_{\rm obs}$ affects the observables and, in fact, the dynamical transition itself becomes possible only when the relaxation times of modes coupled to the iron msd enter the experimental observation window [18, 22]. Therefore, the variance of the slow dispersive motions of the heme iron is not a thermodynamic variable referring to an infinite observation window (in contrast to fast vibrations projecting on $\mathbf{q}$), but a property affected by instrumental resolution [36, 52]. This is reflected by the subscript ">" in Eq. (8) which indicates that $\langle(\delta Q)^2\rangle_>$ is calculated by integrating the response function in Eq. (4) over the frequencies exceeding the observation frequency $\omega_{\rm obs} = \tau_{\rm obs}^{-1}$

$$\langle(\delta Q)^2\rangle_> = \int_{\omega_{\rm obs}}^{\infty}\langle(\delta Q_\omega)^2\rangle(d\omega/\pi). \tag{9}$$

The statistical average over the electrostatic fluctuations can be simplified by a first-order expansion of the potential ϕ_w in x: $\phi_w \simeq \phi_{w,0} - xE_w$, where $\phi_{w,0}$ is the potential at the equilibrium position of the iron and E_w is the electric field projected on $\hat{\mathbf{k}}_0$.

Assuming that E_w is a Gaussian variable, one gets a Gaussian form of $\beta F(x) = x^2/(2\langle(\delta x)^2\rangle)$ where the variance $\langle(\delta x)^2\rangle$ is

$$\langle(\delta x)^2\rangle = \langle(\delta x)^2\rangle_{\rm el}/M_E. \tag{10}$$

Here, the elastic msd

$$\langle(\delta x)^2\rangle_{\rm el} = \langle(\delta q)^2\rangle + \langle(\delta Q)^2\rangle_> \tag{11}$$

is the sum of two statistically decoupled components given, correspondingly, by Eq. (2) and Eqs. (4) and (9). Further, the correction M_E represents the softening of the elastic msd by electrostatic fluctuations of the protein-water interface.

Similarly to the viscoelastic effect, the electrostatic softening depends on the observation window. Accounting again for the frequency cutoff introduced by the finite instrumental resolution, it is given in the form

$$M_E = 1 - (\beta z)^2\langle(\delta x)^2\rangle_{\rm el}\int_{\omega_{\rm obs}}^{\infty} C_E(\omega)d\omega/(2\pi), \tag{12}$$

where $C_E(\omega)$ is the Fourier transform of the time autocorrelation function of the field $E_w(t)$

$$C_E(\omega) = \int_{-\infty}^{\infty}\langle\delta E_w(t)\delta E_w(0)\rangle e^{i\omega t}dt. \tag{13}$$

By applying the fluctuation-dissipation theorem [47] once again, one can recast Eq. (12) in terms of the response function $\chi_E(\omega)$ representing the electrostatic response to an oscillating point dipole $m(t) = m_0\exp(i\omega t)$ placed at the position of the iron atom

$$M_E = 1 - \beta z^2\langle(\delta x)^2\rangle_{\rm el}\int_{\omega_{\rm obs}}^{\infty}\chi''_E(\omega)d\omega/(\pi\omega). \tag{14}$$

In Eq. (14), $\chi''_E(\omega) = {\rm Im}\,[\chi_E(\omega)]$ is the loss function [53].

To summarize, our model for the calculation of the iron msd includes three components. The elastic msd $\langle(\delta x)^2\rangle_{\rm el}$ [Eq. (11)] is the sum of the vibrational [Eq. (2)] and viscoelastic [Eqs. (4) and (9)] components. This elastic msd is affected by the combination of phonon vibrations and the global shape and connectivity of the protein matrix [39]. For charged atoms carrying partial charge z this global elasticity is further softened by the fluctuations of the electric field of the protein-water interface at the position of the atom inside the protein. This softening of displacements of charge z, not incorporated in the global vibrations/deformations affecting $\langle(\delta x)^2\rangle_{\rm el}$, is described by the softening factor M_E in Eq. (14); $M_E = 1$ in Eq. (14) when the atom carries no charge, $z = 0$. Equation (10) also suggests that the interpretation of Eq. (1) as the appearance of a "new" high-temperature mode above T_d is misleading. The electrostatic field of the interface is there even at low temperatures and it is only its fluctuations that are recorded at high temperatures by lifting the kinetic arrest determined by the relative magnitudes of the relaxation time and the instrumental observation window.

III. PARAMETERS OF THE MODEL AND MEAN SQUARE DISPLACEMENT

Here we outline the calculations performed using the model developed in this paper. We need to mention that many parameters entering the model are not experimentally available. Some of them can potentially be extracted from numerical simulations. The usefulness of simulations is, however, limited for interpreting the experimental data since reproducing heterogeneous conditions of partially hydrated protein powders and polycrystals presents significant challenges to simulation protocols [29, 54, 55]. Likewise, the viscoelastic model used here should be viewed as only a first step toward a more realistic description of the elastic response of hydrated proteins. Global motions of proteins are more complex than spherically-symmetric breathing vibrations [39]. However, one of the major conclusions of this paper is the dominance of electrostatics and a relatively small effect of viscoelastic motions on the iron displacements. This observation puts high priority to the development of the electrostatic component of the model, and makes the limitations of modeling the viscoelastic response less critical.

A. Viscoelastic response

The viscoelastic response functions entering Eq. (3) were taken in the Maxwell form [47]

$$\begin{aligned}\Delta K_p(\omega) &= \frac{\Delta K_p i\omega\tau_p}{1+i\omega\tau_p},\\ \mu_w(\omega) &= \frac{G_\infty i\omega\tau_w}{1+i\omega\tau_w}.\end{aligned} \tag{15}$$

In this equation, $\Delta K_p = K_{p,\infty} - K_{p,0}$ is the change in the bulk protein modulus between infinite and zero frequencies and G_∞ is the high-frequency shear modulus of water; $\tau_{p,w}$ are the corresponding relaxation times.

The protein relaxation time $\tau_p(T)$ in Eq. (15) was obtained from measurements done on dry protein powders [30]. The relaxation process in dry proteins is too slow to enter the observation window of the spectrometer and $\Delta K_p(\omega) \simeq \Delta K_p$ in Eq. (15). This observation implies that the frequency dependence of the moduli, e.g., Debye vs dispersive relaxation, does not significantly affect the outcome of the calculations and only $\Delta K_p(T)$ matters for the protein component of the viscoelastic msd. This latter function (listed in the caption of Fig. 2) was obtained to match the experimental intrinsic compressibility [44] of myoglobin [38] $\beta_T = 11.04$ Mbar^{-1} at $T = 298$ K and the temperature variation of Young's moduli of myoglobin crystals at lower temperatures [59, 60] (inset in Fig. 2). An estimate of the myoglobin compressibility using fluctuations of its gyration radius from MD simulations described below [61] leads to $\beta_T = 10$ Mbar^{-1} for $R = 18$ Å calculated from the protein van der Waals volume. This comparison suggests that radial breathing vibrations of an effective sphere are mostly responsible for the volumetric fluctuations of the protein.

From the Maxwell equation, one gets the shear viscosity $\eta_w(T) = G_\infty(T)\tau_w(T)$ which is well tabulated down to the water nucleation temperature [56]. The shear relaxation time $\tau_w(T)$ was obtained from $\eta_w(T)$ and $G_\infty(T)/\text{GPa} = 1.68 - 0.0127(T - 273)$ taken from Ref. 57. The resulting $\tau_w(T)$ turns out to be close to the exponential relaxation time of the longitudinal modulus extracted from inelastic x-ray scattering [58]: $\tau_\ell(T)/\text{s} = 0.84\times10^{-15}\exp(1910\text{ K}/T)$.

The response function in Eq. (3) combined with the dynamic moduli from Eq. (15) can be used to parametrize the viscoelastic response on protein's intrinsic compressibility [44]. For a given instrumental resolution, one obtains from Eq. (3) for the isothermal compressibility $\beta_T \propto \langle(\delta V_p)^2\rangle$ of the protein

$$\beta_T = -(6/\pi)\int_{\omega_{\rm obs}}^{\infty} \text{Im}\left[3\Delta K_p(\omega) + 4\mu_w(\omega)\right]^{-1}(d\omega/\omega). \tag{16}$$

In Fig. 2 we show $\beta_T(T)$ for the parameters adopted in the calculations of the iron msd in Fig. 1 and several values of $\omega_{\rm obs}$. The intrinsic compressibility of the protein rises sharply at the point close to protein's glass tran-

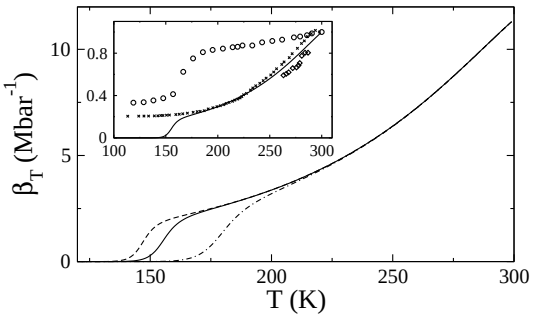

FIG. 2. Intrinsic isothermal compressibility $\beta_T(T)$ of myoglobin calculated from Eq. (16) with $\omega_{\rm obs} = 1$ (dashed line), 10^2 (solid line), and 10^3 MHz (dash-dotted line). The protein and water parameters are those adopted for the calculation of the myoglobin msd, with $\Delta K_p(T)/\text{GPa} = 3.22 - 0.03 \times (T - 298) + 0.00025 \times (T - 298)^2$ obtained to fit the protein intrinsic compressibility at 298 K [38] and the temperature dependence of Young's moduli (crosses in the inset). The inset shows experimental expansivity of the hydration shell of lysozyme (circles) [62], experimental inverse Young's moduli of myoglobin crystals exposed to air of 95–100% (diamonds) [60] and 75% humidity (crosses) [59]. The solid line in the inset shows $\beta_T(T)$ calculated from Eq. (16) at $\omega_{\rm obs} = 10^2$ MHz; all curves in the inset are normalized to the corresponding values at $T = 298$ K.

sition T_g. The latter depends on the observation window, but is close to reported values $T_g \simeq 180 \pm 15$ K [60, 62, 63] marked by breaks in several observable parameters [63]. The rise of compressibility at T_g is caused by the water component of the viscoelastic response function when the relaxation time τ_w becomes smaller than $\tau_{\rm obs} = \omega_{\rm obs}^{-1}$. This onset is also consistent with the glass transition of the hydration shell expansivity [62] shown by open circles in the inset in Fig. 2. The temperature T_g therefore marks the rise in the compressibility of the protein-water interface driven by lifting the dynamical arrest of the water shear response.

The protein and water dynamic moduli tabulated on the protein volumetric data can next be used to calculate the elastic msd in Eq. (11). Its first, phonon component $\langle(\delta q)^2\rangle$ was calculated from the VDOS of metmyoglobin powders from phonon-assisted Mössbauer measurements [7, 9, 26] (dashed lines in Fig. 1). When the viscoelastic component $\langle(\delta Q)^2\rangle_>$ is added to $\langle(\delta q)^2\rangle$ one obtains the elastic msd $\langle(\delta x)^2\rangle_{\rm el}$ shown by the dash-dotted lines in Fig. 1.

The elastic msd in the inset in Fig. 1 shows an upward increase at the highest temperatures studied. It is projected on a similar increase in $\langle(\delta x)^2\rangle$ in the main panel in Fig. 1 and reflects pre-melting of myoglobin crystals when their Young's moduli approach zero [60]. Since the melting temperature is typically higher in protein powders [60], $\Delta K_p(T)$ obtained from fitting the crystal data might overestimate the pre-melting effects. Nevertheless, the temperature dependence of $\Delta K_p(T)$ has a minor effect on either $\langle(\delta x)^2\rangle_{\rm el}$ or $\langle(\delta x)^2\rangle$. The dotted line in the main panel in Fig. 1 shows $\langle(\delta x)^2\rangle$ obtained with a temperature-independent $\Delta K_p = 3.2$ GPa fixed to its value at 298 K, while the dotted line in the inset shows $\langle(\delta x)^2\rangle_{\rm el}$ calculated under the same assumption. The solid and dotted lines in the main panel in Fig. 1 are sufficiently close to each other and are mostly within the experimental uncertainties.

B. Electrostatic response

The theory as formulated so far does not make any specific assumptions about the electric field response function $\chi_E(\omega)$ and any such function obtained from computer or laboratory experiment can be used in Eq. (14). A model of $\chi_E(\omega)$ can be constructed by solving the material Maxwell's equations for the heme immersed in the heterogeneous dielectric formed by the protein and its hydration layer. However, the assignment of the dielectric constants to both the protein and the thin layer of water surrounding proteins is subject to significant uncertainties [32–34]. On the other hand, the simulations of the hydrated myoglobin [61] which we discuss below show that, despite the obvious complexity of the protein-water interface, a Debye form, characterized by only two parameters, fits the simulated loss function $\chi''_E(\omega)$ quite well. We will therefore start our discussion with a phenomenological description aimed to establish whether electrostatic fluctuations can produce a significant effect on the msd under a reasonable set of assumptions. The results of fitting the Debye loss function to reproduce the experimental msd are then compared to MD simulation data.

The dielectric response to charges immersed in a polar medium is dominated by longitudinal modes of dipolar polarization [64] characterized by the dielectric modulus $\epsilon(\omega)^{-1}$, where $\epsilon(\omega)$ is the complex, frequency-dependent dielectric constant of the protein-water mixture. The dielectric response function $\chi_E(\omega)$ establishes the reaction field of the dielectric medium in response to a probe dipole placed at the position of the heme iron. It scales as the inverse cube of the characteristic size d of the heme. The loss function $\chi''_E(\omega)$ can therefore be written in the form

$$\chi''_E(\omega) = \frac{1}{d^3}\ \frac{\epsilon''(\omega)}{|\epsilon(\omega)|^2}. \tag{17}$$

Assuming the Debye form for $\epsilon(\omega) = \epsilon_\infty + (\epsilon_s - \epsilon_\infty)/(1 - i\tau_D\omega)$ one gets

$$\beta z^2 \chi''_E(\omega) = \frac{1}{\delta^2}\ \frac{\omega\tau_L}{1 + (\omega\tau_L)^2}, \tag{18}$$

where δ, $\delta^{-2} = \beta z^2 c_0/d^3$ is a length parameter and $c_0 = \epsilon_\infty^{-1} - \epsilon_s^{-1}$ is the Pekar factor [65]. In addition, $\tau_L = (\epsilon_\infty/\epsilon_s)\tau_D$ is the longitudinal dielectric time and τ_D is the Debye relaxation time [66]; ϵ_∞ and ϵ_s are the high-frequency and static dielectric constants, respectively.

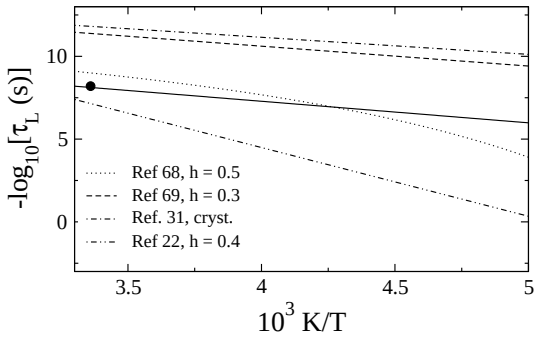

FIG. 3. Dielectric longitudinal relaxation time $\tau_L(T) = (\epsilon_\infty/\epsilon_s)\tau_D(T)$ obtained from Debye relaxation times $\tau_D(T)$ reported in the literature [22, 68, 69] with the protein hydration levels indicated in the legend. The results from Ref. 22 refer to myoglobin confined in PVA, results from Ref. 31 are for metmyoglobin crystals, and Refs. 68 and 69 refer to metmyoglobin powders. The solid line shows relaxation time $\tau_E(T)/\mathrm{s} = 3.2\times10^{-13}\exp[3000\ \mathrm{K}/T]$ of the reaction field response function $\chi_E(\omega)$ [with τ_L replaced with τ_E in Eq. (18)] used to fit the experimental msd [7] shown by closed points in Fig. 1. The closed circle shows $\tau_E(300\ \mathrm{K})$ from MD simulations of hydrated metmyoglobin.

Dielectric properties of partially hydrated proteins have not been well characterized since the results are strongly affected by both the sample preparation and the hydration level. Even dielectric relaxation times measured on samples of close hydration level are rather inconsistent. This point is illustrated in Fig. 3 where the results for partially hydrated myoglobin powders of hydration level $h = 0.3-0.5$ (in g of water per g of protein) have been assembled [22, 67–69]. We also show measurements done on myoglobin crystals [31] for the sake of comparison. Multiple relaxation processes are common for such measurements, and the fastest relaxation, commonly attributed to the hydration shell [30, 68], is shown in Fig. 3.

Even if we could firmly establish the proper relaxation time for the the sample dipole moment, this would not necessarily give us the relaxation time of the reaction field correlation function $\chi''_E(\omega)$, which is in principle accessible experimentally from the Stokes shift dynamics [70]. Because of the linear scaling of the dipole moment variance with the number of dipoles, dielectric measurements emphasize the effect of outer solvation shells, while $\chi''_E(\omega)$ is dominated by waters closest to the probe dipole (heme's iron). This response function thus weighs medium modes into the overall response differently from the dielectric signal [71, 72]. In view of these uncertainties, we have constructed the temperature-dependent relaxation time $\tau_E(T)/\mathrm{s} = 3.2\times10^{-13}\exp[3000\ \mathrm{K}/T]$ (solid line in Fig. 3) which replaces $\tau_L(T)$ in Eq. (18). This relaxation time and $\delta = 0.12$ Å are used in the calculation shown in Fig. 1.

The relaxation time $\tau_E(T)$ used in the fitting is generally consistent with $\tau_L(T)$ from dielectric measurements and, in addition, the Arrhenius slope of $\tau_E(T)$ matches our simulations of the protein Stokes-shift dynamics at elevated temperatures [73]. The same activation energy of $\simeq 3000$ K was used in Doster's analysis [19]. More detailed calculations might require replacing one-relaxation Debye dynamics in Eq. (18) with dispersive dynamics characterized by a distribution of relaxation times, as suggested by the NMR experiment [74].

Substituting Eq. (18) into Eq. (14) one gets for the vibrations softening factor

$$M_E = 1 - \langle(\delta x)^2\rangle_{\mathrm{el}}/(\pi\delta^2)\cot^{-1}\left[\omega_{\mathrm{obs}}\tau_E\right]. \qquad (19)$$

This relation is clearly distinct from other instrumental resolution functions previously suggested in the literature [19, 62]. This function is then used in Eq. (11) to scale the elastic msd $\langle(\delta x)^2\rangle_{\mathrm{el}}$. The result is shown by the solid line in Fig. 1. This calculation thus incorporates all three components of the model: (i) normal mode vibrations, (ii) viscoelastic shape deformation, and (iii) local softening of the displacements of charge z. In contrast, the calculation neglecting the viscoelastic component $\langle(\delta Q)^2\rangle_>$ is shown by the bold dashed line in Fig. 1.

C. Comparison to MD simulations

The function $\beta z^2\chi''_E(\omega)$ required to fit the experimental msd [Eq. (18)] is shown by the dashed line in Figure 4 and compared to the same function obtained from MD simulation of the fully hydrated metmyoglobin [61] (solid line marked as "P+W" in Fig. 4). The height of the maximum quantifies the variance of electric field fluctuations at the iron atom, and it is clearly not overestimated in our fit of the experimental msd. Further, the relaxation time of 6.3 ns of the essentially Debye overall function $\chi''_E(\omega)$ is close to $\tau_E(300\ \mathrm{K}) \simeq 7$ ns in Eq. (18) adopted in the fitting of the experimental msd (closed circle and solid line in Fig. 3). There is therefore a good match between the response function produced by fitting the experimental data and the one obtained directly from MD simulations.

It turns out that protein charges alone can produce fluctuations of the electric field sufficient to reproduce the observed high temperature excess of the iron msd (cf. the lines marked as "P" and "F" in Fig. 4). It is therefore quite possible that the primary role of water in partially hydrated powders is to ionize the surface residues of the protein and plasticize its motions above T_g (Fig. 2). Water in patches solvating ionized residues is strongly coupled to the protein both electrostatically and by surface hydrogen bonds [75]. The fluctuations of the water dipoles could be reduced to motions of domains formed around ionized surface residues and pushed by low-frequency protein motions. Fast water subsystem follows essentially adiabatically protein's motions [76] and their relaxation times are therefore close to each other (Fig. 4). The experimentally observed match between

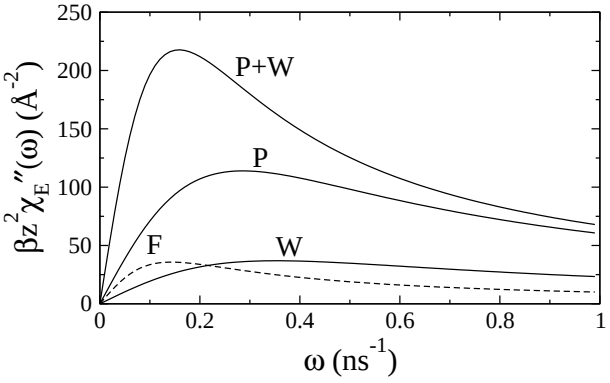

FIG. 4. The loss function $\beta z^2 \chi_E''(\omega)$ obtained from the fitting of the experimental msd to Eqs. (10), (14), and (18) (marked as "F") and from direct MD simulations of the electric field acting on the iron of metmyoglobin. The plot shows the result for the overall electric field produced by protein and water ("P+W") and by protein ("P") and water ("W") separately. The simulation trajectories of 45 ns long, 35 ns of which were used for collecting the correlation functions, were obtained for metmyoglobin solvated by $\simeq 32000$ waters at $T = 300$ K [61].

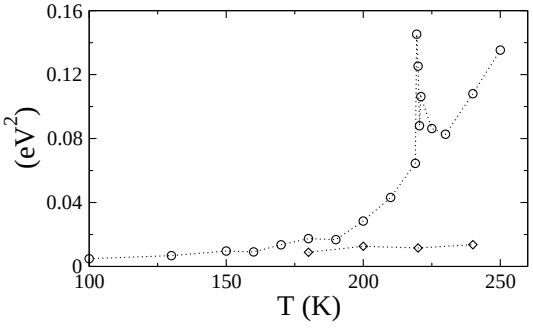

FIG. 5. Variance of the water's electrostatic potential at the active site, $\Delta q^2 \langle (\delta\phi)^2 \rangle$ of the protein plastocyanin from MD simulations (circles) [79]. Diamonds show the difference of water potentials in equilibrium with the active site carrying charges q_1 and q_2, $\beta^{-1}\Delta q(\langle\phi\rangle_1 - \langle\phi\rangle_2)$, $\Delta q = q_2 - q_1$. This latter quantity is sensitive to high-frequency ballistic modes of the hydration water, but not to collective fluctuations of the shell dipole [80]. The two calculations coincide in the linear response approximation, which is valid at low temperatures, below T_d. Linear response breaks down when the collective mode of water's dipolar polarization enters the observation window fixed by the length of the simulation trajectory. The spike at $\simeq 220$ K in the potential variance carries signatures of a weak first-order transition, but its origin is currently unclear.

temperatures of dynamical transition of the water and protein components [15–17] then gains a natural explanation in this picture.

The collective dynamics of the electrostatic fluctuations, in the range of nanoseconds, are slow compared to the sub-picosecond one-particle dynamics [76] even at the room temperature. The electric field dynamics are slow also in comparison with the collective dynamics of the overall dipole of the sample typically reported by dielectric spectroscopy ($\tau_E \simeq 6$ ns vs $\tau_D \simeq 5$ ps from MD simulations at 300 K). One therefore does not need a super-Arrhenius temperature dependence of the relaxation time to connect the sub-picosecond single-molecule dynamics at room temperature to the instrumental resolution window $\simeq 140$ ns near $T_g \simeq 180$ K, as is required by models based on water translations to drive the transition [28, 29, 62]. An Arrhenius temperature dependence with a relatively gentle slope of ~ 3000 K is sufficient to achieve the kinetic arrest at T_g.

IV. DISCUSSION

The picture presented here assigns an increase in the protein msd at the dynamical transition to the entrance of a collective relaxation time of the protein-water interface into the observation window of the spectrometer [22, 30, 77]. We consider two types of interfacial fluctuations, elastic modes changing the global shape of the protein and electrostatic fluctuations. Electrostatics turn out to be the main factor affecting the high-temperature portion of the msd.

The relaxation time of the electric field fluctuations, $\tau_E(T)$, determines the transition temperature by the condition $\omega_{\rm obs}\tau_E(T_d) \simeq 1$. With the Arrhenius form for $\tau_E(T)$, this condition predicts a logarithmic dependence of T_d on the observation frequency,

$$T_d \propto |\ln[\omega_{\rm obs}\tau_0]|^{-1}\,, \qquad (20)$$

where τ_0 is the preexponent in $\tau_E(T)$. For instance, with the observation window of neutron scattering of $\simeq 500$ ps and of Mössbauer spectroscopy of 140 ns, the above equation yields 1.4 for the ratio of T_d values measured by neutron and Mössbauer techniques ($\tau_0 = 10^{-13}$ s). This estimate assumes equal electrostatic relaxation times for (mostly surface) protons and the heme iron, which is likely not true. The actual picture is also more complex as several slope changes contribute to the overall temperature dependence of the msd [78]. It is also the case with the present model producing two different onsets arising from viscoelastic and electrostatic fluctuations: the viscoelastic onset falls in the common range of glass-transition temperatures, $T_g \simeq 180 \pm 15$ K, while the electrostatic onset is in the range assigned to $T_d \simeq 200 - 240$ K.

An increase in T_d was also reported for proteins solvated in glycerol and in concentrated sucrose-water solutions [18]. Although an increase in viscosity does shift T_d in the right direction according to Eq. (20), the alteration of the effective polarity of the hydration layer and the surface charge distribution of the protein might be other factors contributing to the shift. Generally, the present model predicts a decrease in the protein atomic displacements for hydration in solvents of lower polarity.

The main physical question looming behind the phenomenon of the dynamical transition is what are the

mechanisms and physical modes allowing high atomic msd of proteins at physiological temperatures. We emphasize here electrostatic fluctuations as the primary origin of the increase in the protein's atomic displacements. This mechanism connects the translational manifold of the protein's interior to the fluctuations of the more mobile protein-water interface. While this connection was established empirically by experiment [22] [Eq. (1)], numerical simulations directly show the same basic phenomenology for the electrostatic fluctuations and the atomic msd.

Figure 5 shows the results of numerical simulations for the variance of the electrostatic potential produced by the water hydration shell at the active site of the protein plastocyanin [79]. A break in the temperature dependence at T_d refers to the time-scale of $\simeq 10$ ns fixed by the length of the simulation trajectory. The difference of the first moments of the potential in the two redox states of the protein (diamonds in Fig. 5) gives the component of the same property produced by ballistic dynamics of the hydration shell and not sensitive to its collective relaxation [80]. In a sense, the diamonds in Fig. 5 are analogs to the diamonds in Fig. 1 referring to the vibrational component of the msd [7]. There is a clear qualitative similarity between laboratory and numerical results presented in Figs. 1 and 5.

Because the response function of the water's electric field scales as d^{-3} with the distance d from the surface inside the protein, interfacial fluctuations will mostly affect protein's surface residues. The vibrations of the surface protons will therefore be softer than of interior protons [29], and they will stronger contribute to the msd recorded by neutron scattering. There is also a possibility of "surface melting" when $M_E = 0$ in Eq. (10) is reached with rising temperature for a group of atoms. The low-temperature conformation of the corresponding residues will become unstable, with instability released through a conformational transition.

The present model makes several testable predictions. First, the softening of atomic displacements due to the parameter M_E in Eqs. (10) and (14) scales with the squared charge of the atom. In case of heme iron this implies higher msd for a protein in the oxidized state compared to the reduced state. This prediction qualitatively agrees with experiment [81, 82]. One can additionally envision several charge configurations affecting the overall value of the electric field variance at the position of iron. Since electric field is nearly a Gaussian variable, the variance is expected to be simply connected to the average magnitude, $\sqrt{\langle(\delta E)^2\rangle} = (3\pi/8)^{1/2}\langle E\rangle$. The latter is generally a sum of the water (w) and protein (p) fields, $\langle E\rangle = \langle|\mathbf{E}_w + \mathbf{E}_p|\rangle$. The two components can superpose constructively, as in the case of metmyoglobin (Fig. 4), or destructively. Given that iron is positively charged and the overall charge of metmyoglobin at pH= 7 is -2, the destructive superposition of the protein and water electric fields might be achieved for a positively charged myoglobin. In that case, a lower overall field will lead to lower high temperature excess of the msd, a proposal directly accessible to experimental testing.

V. CONCLUSIONS

The model proposed here treats high-temperature atomic displacements of the protein as a combination of viscoelastic deformation of the global protein shape and electrostatic fluctuations coupled to the atomic charge. We suggest that electrostatic fluctuations dominate the high-temperature excess of protein's atomic displacements.

ACKNOWLEDGMENTS

This research was supported by the National Science Foundation (CHE-0910905). CPU time was provided by the National Science Foundation through TeraGrid resources (TG-MCB080116N). We are grateful to Alexei Sokolov, Jan Swenson, and Guo Chen for communicating results of their dielectric measurements to us. DVM has greatly benefited from useful discussions with Hans Frauenfelder, Robert Young, and Alexei Sokolov. Banu Ozkan kindly performed ENM calculations of metmyoglobin and David LeBard helped with the analysis of the MD simulation results.

[1] F. Parak and H. Formanek, Acta Crystallogr. A **27**, 573 (1971).
[2] W. Doster, S. Cusack, and W. Petry, Nature **337**, 754 (1989).
[3] G. Caliskan, R. M. Briber, D. Thirumalai, V. Garcia-Sakai, S. A. Woodson, and A. P. Sokolov, J. Am. Chem. Soc. **128**, 32 (2006).
[4] F. Gabel, D. Bicout, U. Lehnert, M. Tehei, M. Weik, and G. Zaccai, Quat. Rev. Biophys. **35**, 327 (2002).
[5] F. G. Parak, Rep. Prog. Phys. **66**, 103 (2003).
[6] H. Frauenfelder, *The Physics of proteins. An introduction to biological physics and molecular biophysics* (Springer, New York, 2010).
[7] F. G. Parak and K. Achterhold, J. Phys. Chem. Solids **66**, 2257 (2005).
[8] M. Diehl, W. Doster, W. Petry, and H. Schober, Biophys. J. **73**, 2726 (1997).
[9] K. Achterhold and F. G. Parak, J. Phys.: Condens. Matter **15**, S1683 (2003).
[10] M. Marconi, E. Cornicchi, G. Onori, and A. Paciaroni, Chem. Phys. **345**, 224 (2008).
[11] K. Hinsen and G. R. Kneller, Proteins **70**, 1235 (2008).
[12] H. Frauenfelder, S. G. Sligar, and P. G. Wolynes, Science **254**, 1598 (1991).

[13] G. Zaccai, Science **288**, 1604 (2000).
[14] V. Kurkal, R. M. Daniel, J. L. Finney, M. Tehei, R. V. Dunn, and J. C. Smith, Chem. Phys. **317**, 267 (2005).
[15] K. Wood, A. Frölich, A. Paciaroni, M. Moulin, M. Härtlein, G. Zaccai, D. J. Tobias, and M. Weik, J. Am. Chem. Soc. **130**, 4586 (2008).
[16] X.-Q. Chu, A. Faraone, C. Kim, E. Fratini, P. Baglioni, J. B. Leao, and S.-H. Chen, J. Phys. Chem. B **113**, 5001 (2009).
[17] S.-H. Chen, M. Lagi, X. Chu, Z. Yang, K. Chansoo, A. Faraone, E. Fratini, and P. Baglioni, Spectroscopy **24**, 1 (2010).
[18] W. Doster, Biochim. Biophys. Acta **1804**, 3 (2010).
[19] W. Doster, Eur. Biophys. J. **37**, 591 (2008).
[20] P. W. Fenimore, H. Frauenfelder, B. H. McMahon, and R. D. Young, Proc. Natl. Acad. Sci. **101**, 14408 (2004).
[21] G. Chen, P. W. Fenimore, H. Frauenfelder, F. Mezei, J. Swenson, and R. D. Young, Phil. Mag. **88**, 33 (2008).
[22] H. Frauenfelder, G. Chen, J. Berendzen, P. W. Fenimore, H. Jansson, B. H. McMahon, I. R. Stroe, J. Swenson, and R. D. Young, Proc. Natl. Acad. Sci. **106**, 5129 (2009).
[23] P. W. Fenimore, H. Frauenfelder, B. H. McMahon, and F. G. Parak, Proc. Natl. Acad. Sci. **99**, 16047 (2002).
[24] M. D. Ediger, C. A. Angell, and S. R. Nagel, J. Phys. Chem. **100**, 13200 (1996).
[25] D. J. Bicout and G. Zaccai, Biophys. J. **80**, 1115 (2001).
[26] K. Achterhold, C. Keppler, A. Ostermann, U. van Bürck, W. Sturhahn, E. E. Alp, and F. G. Parak, Phys. Rev. E **65**, 051916 (2002).
[27] Y. He, P. I. Ku, J. R. Knab, J. Y. Chen, and A. G. Markelz, Phys. Rev. Lett. **101**, 178103 (2008).
[28] M. Tarek and D. J. Tobias, Phys. Rev. Lett. **88**, 138101 (2002).
[29] A. L. Tournier, J. Xu, and J. C. Smith, Biophys. J. **85**, 1871 (2003).
[30] S. Khodadadi, S. Pawlus, J. H. Roh, V. G. Sakai, E. Mamontov, and A. P. Sokolov, J. Chem. Phys. **128**, 195106 (2008).
[31] G. P. Singh, F. Parak, S. Hunklinger, and K. Dransfeld, Phys. Rev. Lett. **47**, 685 (1981).
[32] P. E. Smith, R. M. Brunne, A. E. Mark, and W. F. van Gunsteren, J. Phys. Chem. **97**, 2009 (1993).
[33] T. Simonson and D. Perahia, Faraday Discuss. Chem. Soc. **103**, 71 (1996).
[34] J. W. Pitera, M. Falta, and W. F. van Gunsteren, Biophys. J. **80**, 2546 (2001).
[35] S. Magazù, F. Migliardo, and A. Benedetto, J. Phys. Chem. B **114**, 9268 (2010).
[36] D. V. Matyushov, J. Chem. Phys. **130**, 164522 (2009).
[37] B. M. Leu, Y. Zhang, L. Bu, J. E. Straub, J. Zhao, W. Sturhahn, E. E. Alp, and J. T. Sage, Biophys. J. **95**, 5874 (2008).
[38] K. Mori, Y. Seki, Y. Yamada, and H. M. K. Soda, J. Chem. Phys. **125**, 054903 (2006).
[39] I. Bahar, T. R. Lezon, A. Bakan, and I. H. Shrivastava, Chem. Rev. **110**, 1463 (2010).
[40] M. M. Tirion, Phys. Rev. Lett. **77**, 1905 (1996).
[41] P. Doruker, A. R. Atilgan, and I. Bahar, Proteins: Struct. Funct. Genet. **40**, 512 (2000).
[42] E. Lyman, J. Pfaendtner, and G. A. Voth, Biophys. J. **95**, 4183 (2008).
[43] R. M. Christensen, *Theory of Viscoelasticity* (Dover Publications, Inc., Mineola, N. Y., 2003).
[44] D. P. Kharakoz, Biophys. J. **79**, 511 (2000).
[45] B. M. Leu, A. Alatas, H. Sinn, E. E. Alp, A. H. Said, H. Yavas, J. Zhao, J. T. Sage, and W. Sturhahn, J. Chem. Phys. **132**, 085103 (2010).
[46] L. D. Landau and E. M. Lifshits, *Theory of elasticity* (Elsevier, Amsterdam, 1986) p. 18.
[47] J. P. Boon and S. Yip, *Molecular Hydrodynamics* (Dover Publications, Inc., New York, 1991).
[48] K. S. Singwi and A. Sjolander, Phys. Rev. **120**, 1093 (1960).
[49] T. E. Cranshaw, B. W. Dale, G. O. Longworth, and C. E. Johnson, *Mössbauer spectroscopy and its applications* (Cambridge University Press, Cambridge, 1985).
[50] H. Frauenfelder, *The Mössbauer effect* (W. A. Benjamin, Inc., New York, 1962).
[51] P. M. Chaikin and T. C. Lubensky, *Principles of condensed matter physics* (Cambridge University Press, Cambridge, 1995).
[52] E. W. Knapp, S. F. Fischer, and F. Parak, J. Chem. Phys. **78**, 4701 (1983).
[53] J. P. Hansen and I. R. McDonald, *Theory of Simple Liquids* (Academic Press, Amsterdam, 2003).
[54] D. Vitkup, D. Ringe, G. A. Petsko, and M. Karplus, Nature Struct. Biol. **7**, 34 (2000).
[55] M. Tarek and D. J. Tobias, Biophys. J. **79**, 3244 (2000).
[56] K. R. Harris and L. A. Woolf, J. Chem. Eng. Data **49**, 1064 (2004).
[57] W. M. Slie, J. A. R. Donfor, and T. A. Litovitz, J. Chem. Phys. **44**, 3712 (1966).
[58] G. Monaco, A. Cunsolo, G. Ruocco, and F. Sette, Phys. Rev. E **60**, 5505 (1999).
[59] V. N. Morozov and S. G. Gevorkian, Biopolymers **24**, 1785 (1985).
[60] V. N. Morozov and Y. Y. Morozova, J. Biomol. Struct. Dyn. **11**, 459 (1993).
[61] D. V. Matyushov, J. Phys. Chem. B, submitted(2011).
[62] W. Doster, S. Busch, A. M. Gaspar, M.-S. Appavou, J. Wuttke, and H. Scheer, Phys. Rev. Lett. **104**, 098101 (2010).
[63] S. Khodadadi, A. Malkovskiy, A. Kisliuk, and A. P. Sokolov, Biochim. Biophys. Acta **1804**, 15 (2010).
[64] D. V. Matyushov, J. Chem. Phys. **120**, 1375 (2004).
[65] S. I. Pekar, *Research in electron theory of crystals* (US-AEC, Washington, D.C., 1963).
[66] B. K. P. Scaife, *Principles of dielectrics* (Clarendon Press, Oxford, 1998).
[67] J. Swenson, H. Jansson, and R. Bergman, Phys. Rev. Lett. **96**, 247802 (2006).
[68] G. Schirò, A. Cupane, E. Vitrano, and F. Bruni, J. Phys. Chem. B **113**, 9606 (2009).
[69] M. Bonura, G. Schirò, and A. Cupane, Spectroscopy **24**, 143 (2010).
[70] S. K. Pal and A. H. Zewail, Chem. Rev. **104**, 2099 (2004).
[71] R. Jimenez, G. R. Fleming, P. V. Kumar, and M. Maroncelli, Nature **369**, 471 (1994).
[72] L. Reynolds, J. A. Gardecki, S. J. V. Frankland, and M. Maroncelli, J. Phys. Chem. **100**, 10337 (1996).
[73] D. N. LeBard, V. Kapko, and D. V. Matyushov, J. Phys. Chem. B **112**, 10322 (2008).
[74] S. A. Lusceac, M. R. Vogel, and C. R. Herbers, Biochim. Biophys. Acta **1804**, 41 (2010).
[75] F. Demmel, W. Doster, W. Petry, and A. Schulte, Eur. Biophys. J. **26**, 327 (1997).
[76] B. Halle and L. Nilsson, J. Phys. Chem. B **113**, 8210 (2009).

[77] R. M. Daniel, J. L. Finney, and J. C. Smith, Faraday Discuss. **122**, 163 (2002).
[78] M. Krishnan, V. Kurkal-Siebert, and J. Smith, J. Phys. Chem. B **112**, 5522 (2008).
[79] D. N. LeBard and D. V. Matyushov, Phys. Rev. E **78**, 061901 (2008).
[80] D. N. LeBard and D. V. Matyushov, J. Phys. Chem. B **114**, 9246 (2010).
[81] E. N. Frolov, R. Gvosdev, V. I. Goldanskii, and F. G. Parak, J. Biol. Inorg. Chem. **2**, 710 (1997).
[82] A. M. Jorgensøn, F. Parak, and H. E. M. Christensen, Phys. Chem. Chem. Phys. **7**, 3472 (2005).